RSC Applied Polymers

PAPER

View Article Online
View Journal

Cite this: DOI: 10.1039/d6lp00019c

Mechanical and interfacial properties of zwitterionic hydrogels *via* a high-entanglement network design: a study of monomer and crosslinker synergy

Ying-Chieh Chuang,†[a] Kang-Ting Huang,†[a] Jin-Jia Hu[b] and Chun-Jen Huang*[a,c,d]

Hydrogels with high water content and biocompatibility are attractive for biomedical applications, but generally suffer from poor mechanical strength and limited durability. Recently, the high-entanglement network strategy has emerged as a simple yet powerful approach to enhance hydrogel mechanics by forming densely entangled polymer chains with minimal crosslinking density. In this study, we extend this concept to zwitterionic hydrogels to achieve mechanical resilience, superior adhesion, lubricity and anti-fouling properties. Four sulfobetaine-based monomers, sulfobetaine acrylamide (SBAA), sulfobetaine methacrylamide (SBMAA), sulfobetaine acrylate (SBA) and sulfobetaine methacrylate (SBMA), were polymerized under highly concentrated conditions with crosslinked structures using *N*,*N*′-methylenebisacrylamide (MBAA) or *N*,*N*′-methylenebismethacrylamide (MBMA). Systematic comparison revealed that the monomer structure, hydrogen-bonding capacity, and α-methyl substitution critically influence the polymerization kinetics, network homogeneity, mechanical properties, viscoelasticity, frictional and antifouling behaviors. The resulting zwitterionic hydrogels developed by suitably pairing the monomer and crosslinker exhibited enhanced elasticity, toughness, ultralow friction, good adhesion and antifouling properties under physiological conditions. These findings establish high entanglement as an effective structural design principle for developing mechanically resilient and antifouling hydrogels for biomedical devices and soft material interfaces.

Received 21st January 2026,
Accepted 2nd March 2026

DOI: 10.1039/d6lp00019c

rsc.li/rscapplpolym

Introduction

Hydrogels, which are hydrophilic polymeric networks, possess high water content and biocompatibility, making them promising materials for biomedical applications.[1–3] However, their intrinsic mechanical weakness restricts their practical use in load-bearing environments. Thus, numerous reinforcement strategies have been developed, including interpenetrating polymer networks (IPNs), double-network (DN) structures,[4,5] nanocomposites,[6] and slide-ring[7,8] systems. These approaches enhance the strength and toughness of hydrogels through multiple networks, sacrificial bonds, or energy-dissipating mechanisms. For instance, DN hydrogels combine a brittle first network with a ductile second network to achieve remarkable toughness,[4,5] while nanocomposite and supramolecular hydrogels exploit reversible interactions such as hydrogen bonding, ionic coordination, or hydrophobic association.[6] However, despite these advances, many systems require complex synthesis, produce structural heterogeneity, and involve trade-offs among elasticity, toughness, and swelling.[9,10] Thus, simple and robust design principles remain essential for next-generation hydrogels with balanced mechanical and physicochemical properties.

A highly entangled network strategy was introduced to strengthen hydrogels through physical chain entanglements rather than through dense chemical crosslinking.[11–14] By polymerizing monomers at high concentrations with minimal amount of crosslinker, densely entangled chains form junctions that dissipate energy efficiently while maintaining elasticity and water content. Miyata *et al.* demonstrated that these networks exhibit well-balanced viscoelasticity and extraordinary resilience.[12] Suo *et al.* further revealed that these hydro-

[a]*Department of Chemical & Materials Engineering, National Central University, Jhong-Li, Taoyuan 320, Taiwan. E-mail: cjhuang@ncu.edu.tw*
[b]*Department of Mechanical Engineering, National Yang Ming Chiao Tung University, No. 1001, Daxue Rd. East Dist., Hsinchu City 300093, Taiwan*
[c]*R&D Center for Membrane Technology, Chung Yuan Christian University, 200 Chung Pei Rd., Chung-Li City 32023, Taiwan*
[d]*School of Materials Science and Engineering, The University of New South Wales, Sydney, NSW 2052, Australia*
†Equal contribution.

gels display ultralow friction, up to six-times lower than that of PTFE, owing to their hydrated, extended chains, which produce smooth sliding interfaces.[11] This straightforward approach enables the fabrication of hydrogels combining durability, stretchability, and lubricity without complex synthetic routes or heterogeneous crosslinking structures.

Most reported highly entangled hydrogels are composed of neutral polymers such as polyacrylamide or polyethylene glycol, where charge-free chains readily form entanglements.[11,12,15–17] Extending this concept to ionic or zwitterionic systems presents new challenges and opportunities.[18,19] Charged groups introduce electrostatic interactions, ion-dipole associations, and hydration effects that strongly influence network formation and chain dynamics. Zwitterionic polymers, in particular, show exceptional antifouling and hydration behavior but often suffer from poor mechanical integrity.[20–23] The delicate balance between electrostatic attraction and hydration repulsion may either promote or disrupt chain entanglement. Moreover, the often-overlooked molecular structures of monomers and crosslinkers can significantly influence the backbone rigidity, crosslinking homogeneity, entanglement density, and energy dissipation.[24,25] The synergy between monomers and crosslinkers is governed by their reactivity ratios during radical copolymerization, which dictates whether the resulting network is random, gradient, or blocky in nature.[26,27] The arrangements can significantly influence the local density of entanglements. Accordingly, understanding this interplay is crucial for creating ionic hydrogels that combine mechanical robustness with superior biocompatibility and surface lubricity.

In this work, we extend the high-entanglement concept to zwitterionic hydrogels to overcome their inherent mechanical limitations and clarify the effect of molecular structures on the entanglement-induced mechanical reinforcement. Four sulfobetaine-based monomers, sulfobetaine methacrylate (SBMA), sulfobetaine acrylate (SBA), sulfobetaine acrylamide (SBAA) and sulfobetaine methacrylamide (SBMAA), were synthesized to examine the influence of hydrogen bonding, α-methyl substitution and reactivity on network formation and uniformity (Scheme 1). Crosslinkers, *N*,*N*′-methylenebisacrylamide (MBAA) and *N*,*N*′-methylenebismethacrylamide (MBMA), were employed to regulate the crosslinking density and distribution. By comparing the ionic systems, we elucidate that the charge group, molecular architecture and polymerization kinetics influence their entanglement behaviour and mechanical performance. Surface and antifouling measurements further reveal the impact of polymer entanglement on surface lubricity, adhesion and biofouling re-

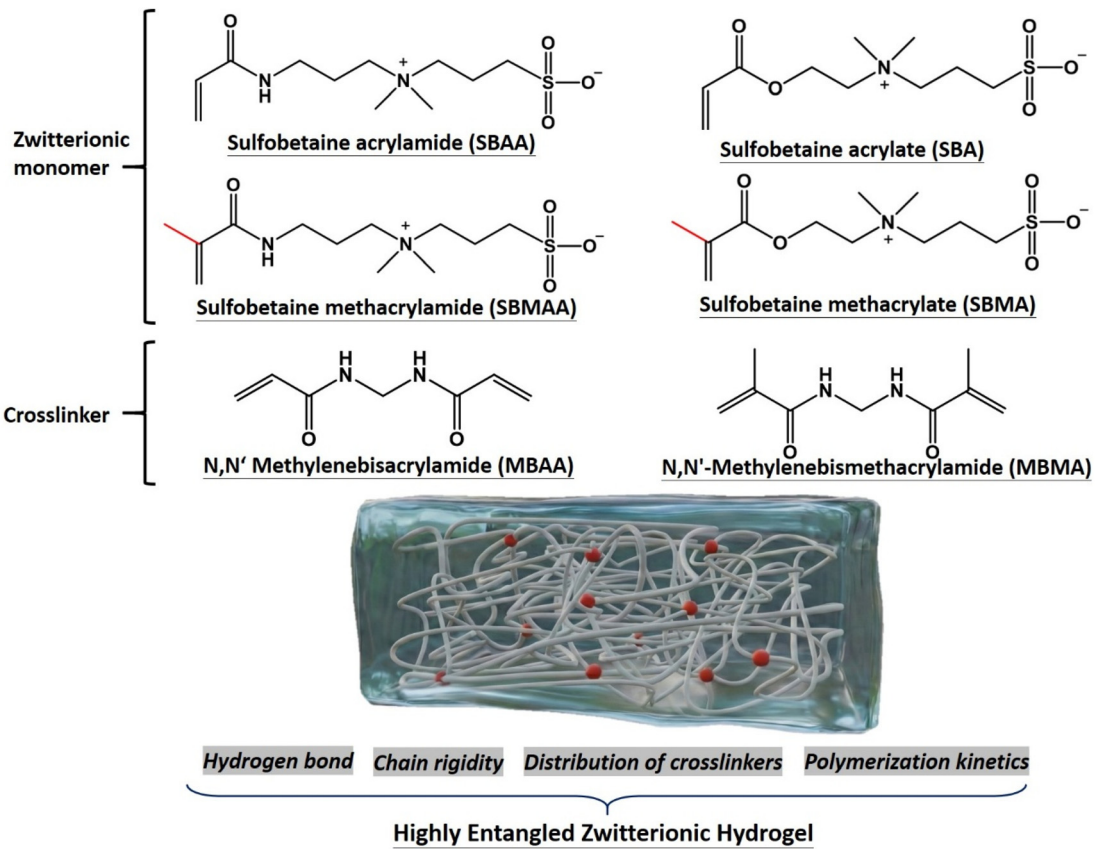

Scheme 1 Zwitterionic monomers, including sulfobetaine acrylamide (SBAA), sulfobetaine methacrylamide (SBMAA), sulfobetaine acrylate (SBA) and sulfobetaine methacrylate (SBMA), and crosslinkers, including *N*,*N*′-methylenebisacrylamide (MBAA) and *N*,*N*′-methylenebismethacrylamide (MBMA), as building blocks for the construction of highly entangled zwitterionic hydrogels (EZHs) and conventional zwitterionic hydrogels (ZHs).

sistance. This study provides design guidelines for the preparation of robust, antifouling, and mechanically and interfacially tunable zwitterionic hydrogels that can be applied in biomedical coatings and soft devices.

Materials and methods

Materials

N-[3-(Dimethylamino)propyl]acrylamide (DAA), *N*-[3-(dimethylamino)propyl]methacrylamide (DMAA), 2-(dimethylamino) ethyl methacrylate (DMA), 2-(dimethylamino)ethyl acrylate (DA), 2-oxoglutaric acid (2-OA), and *N*,*N*′-methylenebismethacrylamide (MBMA) were purchased from Tokyo Chemical Industry (TCI). Sodium chloride and *N*,*N*′-methylenebis(acrylamide) (MBAA) were obtained from Alfa Aesar. Acetone was purchased from TEDIA, and acetonitrile from AENCORE. Fluorescein-5-maleimide was obtained from MCE. 3,3′,5,5′-Tetramethylbenzidine (TMB) was purchased from Thermo Fisher Scientific. Bovine serum albumin (BSA) was obtained from MdBio Inc. Anti-albumin antibody and goat anti-rabbit IgG antibody (HRP-conjugated) were purchased from Arigo Biolaboratories. LB (Luria–Bertani) broth and LB agar were purchased from Neogen Culture Media. Poly(ethylene glycol) dimethacrylate (PEGDMA, M_n = 550 Da) and Tween 80 were purchased from Sigma–Aldrich. The LIVE/DEAD® BacLight™ Bacterial Viability Kit was obtained from Life Technologies. All other reagents were of analytical grade and used as received without further purification.

Synthesis of highly entangled zwitterionic hydrogels (EZH)

The synthetic procedures for the SBA, SBMA, SBAA, and SBMAA monomers are described in the SI. The synthesis of EZHs follows the previous literature.[28] EZHs were prepared by dissolving the photoinitiator (2-OA) in deionized water at a molar ratio of initiator to water of 0.001536 : 1. The crosslinker, MBAA or MBMA, was dissolved separately in deionized water at a crosslinker-to-water molar ratio of 0.00384 : 1. Each solution was purged with nitrogen for 15 min to remove dissolved oxygen and subsequently ultrasonicated for 15 min to degas. The crosslinker and initiator solutions were then mixed at a 1 : 1 volume ratio. The monomers were dissolved in this mixture inside a glove box and poured into Teflon molds. The molar ratio of monomer to water was 1 : 6. Polymerization was initiated under 365 nm UV light (100 mW cm^{-2}) for 20 min. After polymerization, the hydrogel samples were immersed in deionized water for storage.

For the preparation of conventional zwitterionic hydrogels (ZH), the water-to-monomer ratio was 28, the crosslinker-to-monomer molar ratio was 0.32, and the initiator-to-monomer molar ratio was 0.01. The other procedures are identical to that for EZHs.

Kinetics of polymerization

Photopolymerization kinetics were investigated using model monomers of SBMA, SBA, SBAA, and SBMAA at a concentration of 0.3 M, with 2-OA at 0.42 mol% as the photoinitiator. The reactions were carried out under UV irradiation (λ_{max} = 365 nm, 13.2 mW cm^{-2}) in 0.2 M NaCl solution at 25 °C. Real-time samples were collected from sealed glass vials at predetermined intervals and analyzed by ^{1}H NMR spectroscopy (AVANCE III HD 600 MHz NMR, Bruker) after dissolution in 0.5 M NaCl-D_2O. The polymerization profiles showed a short induction period followed by pseudo-first-order kinetics, as indicated by the linear plots of $\ln([M]_0/[M]_t)$ *versus* exposure time (t).

Physicochemical characterization of hydrogels

Mechanical testing. Tensile tests were conducted using a universal testing machine (QC-508M1F, Cometech) under ambient conditions to evaluate the mechanical behavior of the hydrogel samples. The hydrogels were cut into rectangular specimens with dimensions of 20 mm × 10 mm × 2 mm. The tests were performed at a tensile rate of 10 mm min^{-1}. Each sample was first pre-stretched to 3% of its original length, followed by cyclic tensile-release tests at 150%, 200%, 250%, 300%, and 350% of the original length, with a 1 min relaxation between each cycle. The hysteresis behavior was analyzed to assess the energy dissipation capability of the hydrogels.

Rheological measurements. Rheological characterization was performed using a rheometer equipped with a temperature-controlled chamber (MCR 302e, Anton Paar). The instrument applies oscillatory shear deformation of known amplitude and frequency to the sample. Hydrogel samples were cut into square specimens (30 mm × 30 mm × 2 mm). The measurements were conducted at a fixed angular frequency of ω = 1 rad s^{-1}. Amplitude sweep tests were carried out over a strain range of 10–1000% to evaluate the viscoelastic and mechanical behavior of the hydrogels.

FTIR spectroscopy. FTIR spectroscopy (IRSpirit, Shimadzu) identifies functional groups based on the characteristic absorption of infrared radiation by molecular vibrations and rotational transitions in the sample. Before each sample scan, the background spectrum of ambient air was collected. Measurements were performed at a resolution of 4 cm^{-1} over the wavenumber range of 400–4000 cm^{-1}, with 45 scans averaged per sample. The prepared samples were placed on the sample stage and analyzed in reflection mode to identify the characteristic functional groups from their absorption peaks.

Degree of swelling. Hydrogels are highly hydrated three-dimensional polymer networks, and their water-retention capability is a critical parameter for practical applications. The swelling ratio was determined according to ASTM D570. The samples were first dried in an oven for one week, cooled in a desiccator, and weighed (W_d). Then, they were immersed in distilled water at 25 °C for 24 h, removed, blotted with tissue to remove surface water, and reweighed (W_s). The swelling ratio was calculated using eqn (1), as follows:

$$\text{Sweling ratio}\,(\%) = \frac{W_s - W_d}{W_d} \times 100\% \quad (1)$$

where W_s and W_d represent the swollen and dry weights of the hydrogel, respectively.

Toughness was determined as the integrated area under the stress–strain curve obtained from tensile testing. This experiment compares the equilibrium swelling ratios and mechanical property improvements among the hydrogels with four different monomers.

Crosslinking density by compression test. Hydrogels were equilibrated in water at 25 °C prior to measurement. The equilibrated gels were cut into cylindrical specimens (diameter 25 mm, height 10 mm) and tested using a universal testing machine at a compression rate of 10 mm min^{-1}. The compressive modulus (G) was determined from the stress–strain relationship given by eqn (2), as follows:[29–31]

$$\sigma = G(\alpha - \alpha^{-2}) \quad (2)$$

where σ is the compressive stress and α is the ratio of the original to deformed sample thickness. A linear relationship between σ and $(\alpha - \alpha^{-2})$ was observed, and G was determined from the slope.

The effective crosslinking density (ν_e) was then calculated using eqn (3), as follows:

$$G \approx RT\nu_e\phi^{1/3} \quad (3)$$

where R is the gas constant, T is the absolute temperature (K), and ϕ is the polymer volume fraction of the prepared or swollen hydrogel.[29]

Adhesion energy test. Adhesion strength was measured using a universal testing machine in reverse compression mode to quantify the detachment stress between the hydrogels and different substrate surfaces. Hydrogels were synthesized on glass slides modified with 3-(trimethoxysilyl)propyl methacrylate. The hydrogel samples (25 mm × 20 mm × 3 mm) were fixed on the glass substrate and attached to the load cell. The pulling rate was set to 10 mm min^{-1}. The adhesion stress (σ-adhesion) was calculated using eqn (4) and (5), as follows:

$$\sigma_{adhesion} = \sigma_{max} - \sigma_w - \sigma_{deformation} \quad (4)$$

$$\sigma_{deformation} = \Delta L \times G \quad (5)$$

where σ_{max} is the maximum detachment stress, σ_w is the stress due to the weight of the samples, $\sigma_{deformation}$ accounts for the elastic deformation of the gel, and ΔL is the deformation prior to detachment from the substrate surface, as shown in Fig. S1.

Dynamic light scattering (DLS). DLS measurements were performed on a NanoPlus-3 spectrophotometer (Shimadzu Co., Kyoto, Japan). The sample was loaded into a cuvette for measurement. The DLS experiments were conducted at 25 °C with a pinhole aperture of 25 μm and a scattering angle of 165°. The standard deviation of the time-averaged scattering intensity $\langle I \rangle_T$ was calculated to quantify network homogeneity, where a larger standard deviation indicates greater inhomogeneity, whereas a smaller value reflects a more uniform network structure.[29] Scattering intensities were measured at 60 different positions across the hydrogel network.

Atomic force microscopy (AFM). In AFM, a cantilever with a sharp tip detects the interaction forces between the probe and the sample surface. The deflection of the cantilever, monitored *via* a laser reflected onto a position-sensitive photodiode, provides a direct measure of these forces. The spring constant of the AFM cantilever was determined using the method described in the literature.[32] The tip–surface interaction force was then calculated using Hooke's law based on the deflection and spring constant.[33]

AFM (SPI3800N, Hitachi) measurements were performed in force-curve mode using cantilevers (f = 65 kHz, k = 0.5 N m^{-1}; Olympus Corporation, Japan). The instrument parameters were set as FFM = ±1, DIF = 0.1–0.2, and I gain = 0.5. The adhesive force was derived from the force–distance (F–d) curves obtained during approach and retraction. Three points were measured on each sample to calculate the average surface adhesion energy.[34]

Underwater friction test. Underwater friction tests were performed using a custom-built universal testing system. Medical-grade silicone sheets (Shore hardness 60A) were used as substrates. Hydrogels were synthesized on 3-(trimethoxysilyl) propyl methacrylate-modified glass slides and fixed to a movable stage. Deionized water or 0.15 M NaCl solution was added until the liquid fully covered both the hydrogel and substrate. The samples were equilibrated for 10 min to allow complete swelling.

The stage was then translated at a constant speed of 150 mm min^{-1} over a distance of 130 mm, and the dynamic friction coefficient was calculated from the recorded force–displacement data. Each test was repeated 25 times to assess the variations in the dynamic friction coefficient across trials.

Biofouling tests

Bacterial fouling. *Escherichia coli* (*E. coli*) and *Staphylococcus aureus* (*S. aureus*) were cultured in LB broth (10 μL inoculum in 10 mL medium) at 37 °C and 100 rpm for 16 h. The bacteria were harvested by centrifugation (5000 rpm, 5 min) and re-dispersed in PBS to an OD_{600} of 0.15. Hydrogels were incubated in 3 mL of the bacterial suspension at 37 °C and 100 rpm for 3 h. The samples were washed three times with PBS (5 min each) to remove unattached bacteria. Live/dead staining was performed using the LIVE/DEAD® BacLight™ kit for 15 min in the dark, followed by PBS washing. Fluorescence images were obtained using a Nikon ECLIPSE Ts2 microscope at three random locations per sample, and bacterial coverage was quantified using ImageJ software.

Protein fouling. Hydrogels were incubated in BSA solution (4.5 mg mL^{-1} PBS) for 3 h at 37 °C and 100 rpm, then washed three times with PBST (PBS containing 0.05 wt% Tween 80). Subsequently, the samples were incubated with anti-BSA IgG primary antibody (0.125 μL mL^{-1} PBST) for 1 h, washed, and then incubated with HRP-conjugated secondary antibody (0.125 μL mL^{-1} PBST) for 1 h. After washing, 1 mL of TMB substrate was added to each sample for 30 s, and the reaction was quenched by adding 0.5 mL of 1 M H_2SO_4 to yield a yellow solution. The solution (200 μL) was transferred to a 96-well plate, and the absorbance at 450 nm was measured using an ELISA reader (BioTek Synergy™ HT).

Statistical analysis

All data are presented as mean ± standard deviation (SD). Statistical comparisons between groups were conducted using Student's *t*-test. A *p*-value ≤ 0.05 was considered statistically significant.

Results and discussion

Optimization of highly entangled zwitterionic hydrogels

To examine the influence of the α-methyl group and potential hydrogen bonding on the molecular structure and mechanical properties of highly entangled zwitterionic hydrogels, four sulfobetaine-based monomers, SBAA, SBMAA, SBA and SBMA, were synthesized (Scheme 1). The detailed synthetic procedures for the monomers are described in the SI and their ^{1}H NMR spectra were analyzed as shown in Fig. S2–S5, respectively.

The synthesis strategy of highly entangled hydrogels aims to optimize the balance between physical and chemical crosslinking through the combined effects of chain entanglement and covalent bonding.[11,12] The energy dissipation mechanism based on polymer chain entanglement effectively overcomes the limitation of low mechanical strength commonly found in conventional hydrogels. In this study, we adjusted the ratio of the chemical crosslinker to the monomer concentration to construct polymer networks with different degrees of chain entanglement and to determine the optimal formulation for enhanced mechanical performance. In Fig. S6, the molar ratio of photoinitiator to MBAA crosslinker was fixed at $I/C = 0.4$, and the molar ratio of monomer to water (W) at 1 : 6. The toughness of the hydrogels was determined from the area under the stress–strain curves obtained from tensile tests. Comparison among samples with different cross-linker contents revealed that the optimal cross-linker content for all the hydrogels is 0.025, corresponding to a crosslinker-to-water molar ratio of 0.00384 : 1. This enhancement can be attributed to the denser polymer chains in the highly entangled hydrogels and high degree of polymerization between links, which promote physical entanglement and thus improve their mechanical properties. We applied the above formula for development of entangled zwitterionic hydrogels (EZHs) in comparison with conventional zwitterionic hydrogels (ZHs).

As shown in Fig. 1a, tensile tests of the EZH and ZH hydrogels were conducted using a universal testing machine. The entanglement effect markedly improved the mechanical properties of the zwitterionic hydrogels, with their toughness enhanced by approximately 500%–2000%.[11] The comparative values are summarized in Table S1. The improvement in mechanical performance followed the order of SBMA > SBA > SBMAA > SBAA. Although these polymers contain identical zwitterionic pendant groups, the difference may be closely associated with their network formation, chain flexibility, swelling behavior and inter- and intra-chain interactions.

In addition to observing the recoverability of EZHs, we prepared EZHs for reciprocating tensile tests within a strain range of 0% to 200% and under a loading rate of 0.0016 s^{-1}. As shown in Fig. 1b–e, all the EZHs exhibit excellent recoverability and hysteresis was negligible. This can be attributed to the fact that hysteresis in hydrogels primarily arises from the rupture of closed polymer loops around chemical crosslinks.[35] When the crosslinker concentration is too high, excessive chemical crosslinks amplify hysteresis-related defects within the network.

Effects of backbone structures of EZHs on mechanical properties

To reveal the effects of the backbone structure of EZHs on their mechanical properties, we measured the hydrogen bonding, swelling ratio, crosslinking density and distribution, and mesh size of EZHs to elucidate their profound effects on chain entanglement and energy dissipation from the molecular point of view. To verify the presence of intermolecular hydrogen bonding in the hydrogels, Fourier transform infrared spectroscopy (FTIR) analysis was performed, as shown in Fig. 2a–d, respectively. The characteristic amide II absorption peak, a mixed vibration primarily involving N–H bending and C–N stretching, appears at around 1570 cm^{-1}, indicating the presence of intermolecular hydrogen bonding. It was observed that both the ZH and EZH of pSBA and pSBMA hydrogels, respectively, lack hydrogen donors and do not exhibit inter- and intra-molecular hydrogen bonds. In contrast, the pSBAA and pSBMAA hydrogels, which contain both hydrogen donors and acceptors, displayed distinct amide I ($\nu_{C=O}$) and amide II ($\delta_{NH} + \nu_{C-N}$) peaks, confirming the formation of hydrogen bonds. Moreover, the strength of hydrogen bonding can be evaluated based on the wavenumber difference ($\Delta\nu$) between the amide I and amide II peaks; a smaller $\Delta\nu$ corresponds to stronger hydrogen bonding interactions.[36] Generally, a $\Delta\nu$ of 176 cm^{-1} or less is indicative of hydrogen bonding.[36,37] In this study, the ZH and EZH of pSBAA and pSBMAA, respectively, exhibited a $\Delta\nu$ of 72 cm^{-1}, providing clear evidence for the presence of strong hydrogen-bond interactions. Moreover, the strength of hydrogen bonding did not increase with network entanglement. This should be attributed to geometric constraints, such as the bond length and angle between the hydrogen donors and acceptors, which can significantly influence the hydrogen bond strength.[38,39]

We evaluated the swelling behavior of the hydrogels in deionized (DI) water and compared the swelling ratios of EZHs with those of ZHs. As shown in Fig. 2e, the swelling ratios of ZHs ranged from 5% to 35%, whereas those of EZHs were significantly higher, ranging from 90% to 160%. The pronounced increase in swelling arises from the reduced number of restrictive chemical crosslinking points in the highly entangled networks, which allows the polymer chains to expand more freely.[40,41]

Additionally, we examined the effect of molecular structure on the swelling behavior of EZHs, as shown in Fig. 2e. The hydrogels capable of forming inter- and intra-molecular hydrogen bonds (pSBAA and pSBMAA) exhibited higher swelling ratios than those lacking hydrogen-bonding capability (pSBA

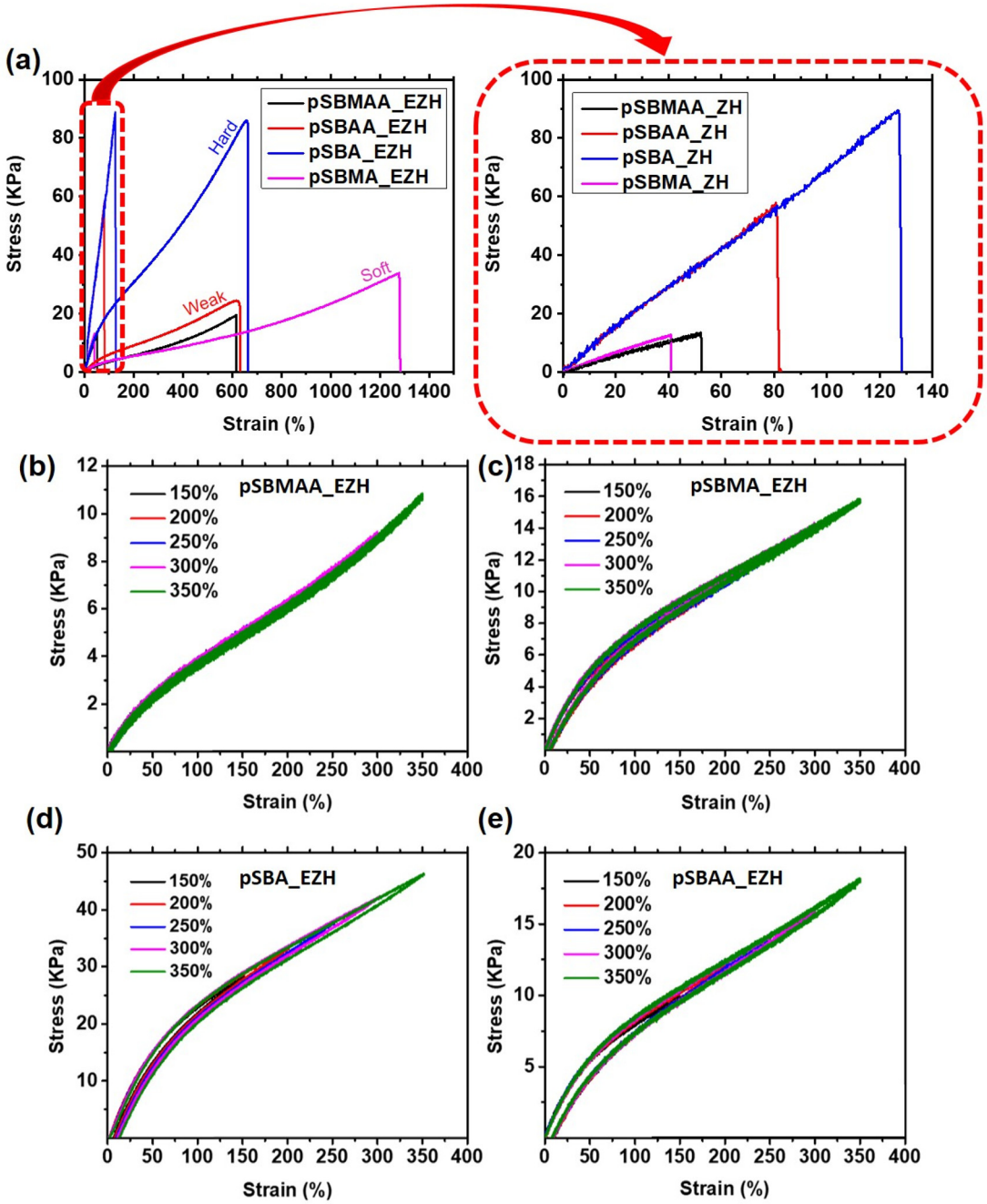

Fig. 1 (a) Tensile tests of EZH and ZH hydrogels. The 0–140% strain region is shown in the magnified inset. Reciprocating tensile tests with a strain in the range of 0% to 200% and under a loading rate of 0.0016 s^{-1} for recoverability of EZHs of (b) pSBMAA, (c) pSBMA, (d) pSBA and (e) pSBAA.

and pSBMA). The enhancement results from the improved hydration facilitated by hydrogen bonding. Additionally, the hydrogels containing an α-methyl group showed lower swelling ratios due to the increased hydrophobicity imparted by the methyl substituent.[42] An inverse correlation was observed that the hydrogels with higher swelling ratios showed smaller improvements in mechanical strength (Fig. 1a). The higher swelling typically dilutes the density of polymer chains, leading to swelling-weakening behavior.[43,44] Because the mechanical performance of highly entangled hydrogels with fewer chemical crosslinking points relies heavily on physical entanglements, they experience exceptionally high swelling and therefore exhibit an even stronger dependence of mechanical properties on swelling.

Network uniformity analysis

The formation of networks is critical in the mechanical performance of hydrogels. Thus, in this work, we evaluated the reactivity of each monomer under identical conditions. The monomer conversion at various time points within 90 min was

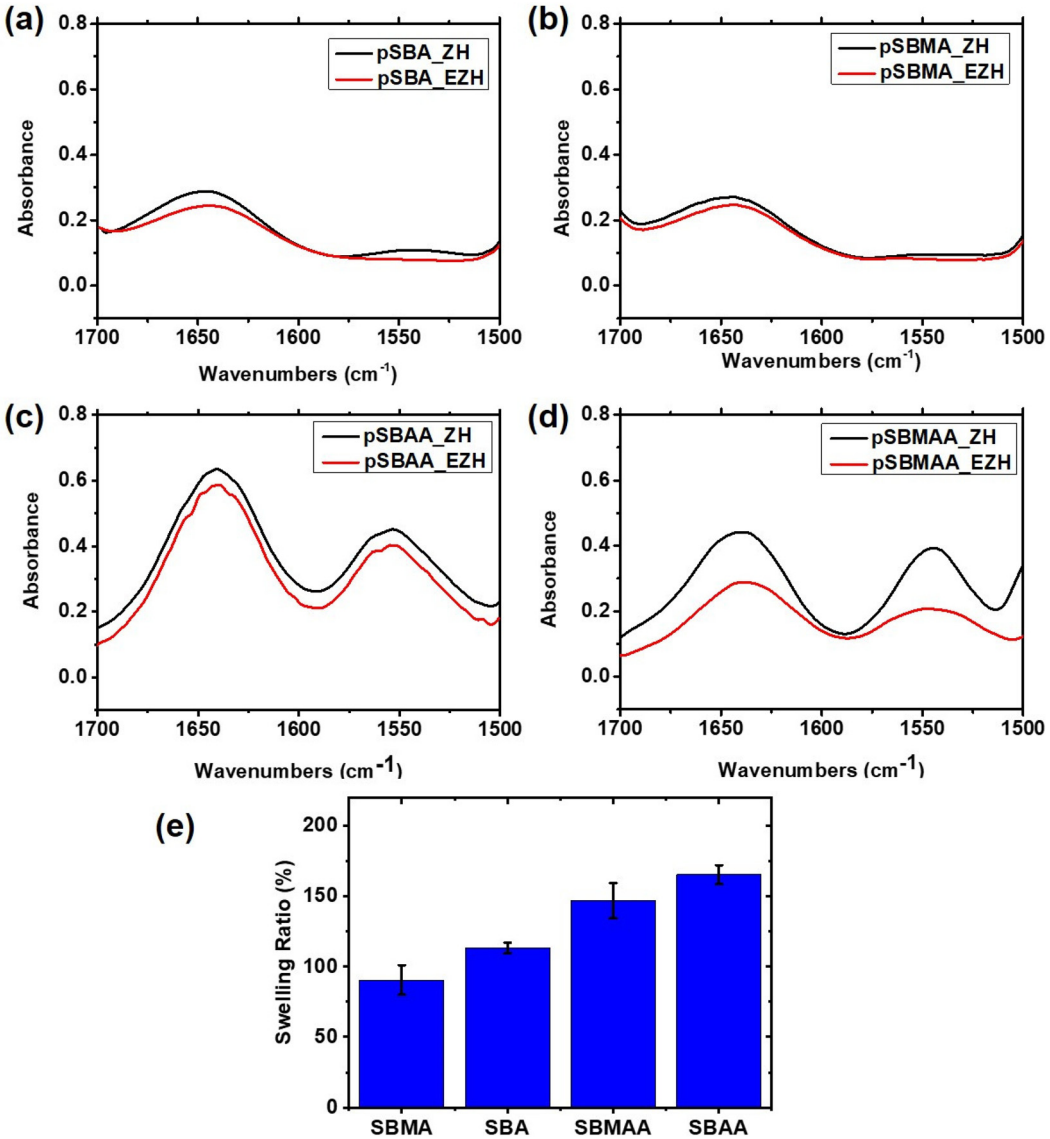

Fig. 2 Fourier-transform infrared spectroscopy (FTIR) analysis to examine intermolecular hydrogen bonding in conventional and highly entangled zwitterionic hydrogels of pSBA (a), pSBMA (b), pSBAA (c) and pSBMAA (d). Swelling ratios of all the EZHs (e).

quantified using NMR, and the apparent rate constant (K_{app}) was calculated. As shown in Fig. 3a, pseudo-first-order polymerization kinetics were observed for all the monomers. The reactivity follows the order of SBA > SBAA > SBMA > SBMAA. The monomers containing an α-methyl group (SBMA and SBMAA) exhibited significantly lower reactivity than their non-α-methyl counterparts (SBA and SBAA), respectively.[45] Furthermore, the acrylamide-based monomers showed slightly lower reactivity than the acrylate analogues. This behavior is due to the weaker internal rotational constraints around the C–C bond between the backbone and the amide moiety. In acrylates, stronger interactions between the backbone radicals and pendant carbonyl groups impose greater rotational hindrance compared with interactions involving amide groups.[45]

To examine how differences in monomer and crosslinker reactivity influence network uniformity, we utilized two crosslinkers for developing EZHs, which are MBAA and MBMA without and with an α-methyl group, respectively (Scheme 1). The amide-based crosslinkers offer distinct internal rotational constraints and hydrogen-bonding potential, which help clarify the structural synergy we aimed to study. Hydrogels were synthesized using monomer-crosslinker pairs with matched or mismatched reaction rates. DLS was employed to measure scattering intensity, and the standard deviation was used as an index of network heterogeneity (Fig. 3b).[29,46] The EZHs formed from fast-reacting monomers paired with fast-reacting crosslinkers (*e.g.*, SBA or SBAA with MBAA) exhibited a lower standard deviation, indicating more uniform networks. Similarly, slow monomers (SBMA or

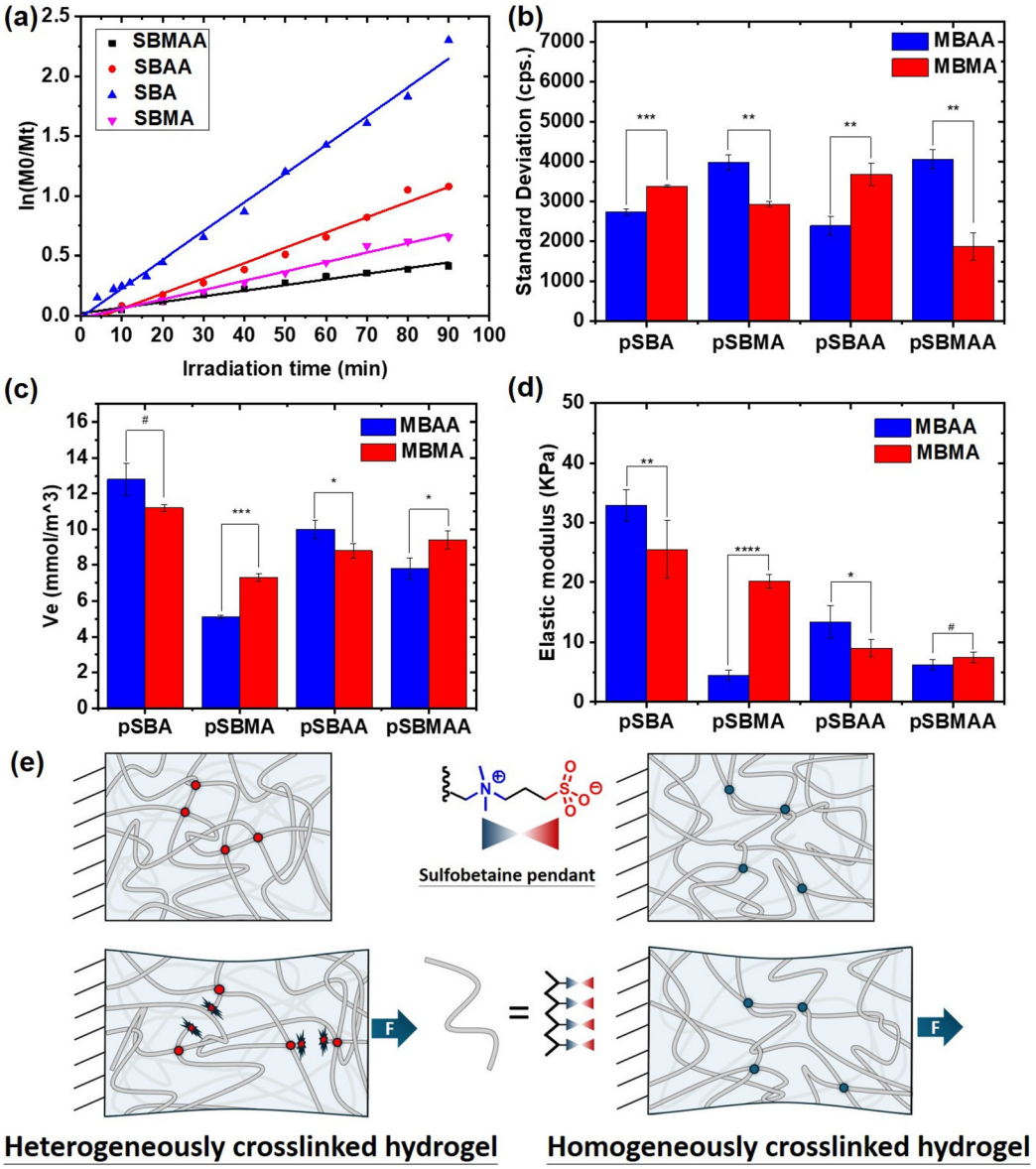

Fig. 3 (a) Semi-logarithmic kinetic plot and conversion curves for zwitterionic monomers. (b) Comparison of light-scattering intensity standard deviations for EZHs with a crosslinker of MBAA or MBMA. (c) Crosslinking densities (V_e) of EZHs with a crosslinker of MBAA or MBMA. (d) Elastic modulus of EZHs with a crosslinker of MBAA or MBMA (n = 3; #p > 0.05, *$P \leq 0.05$, **$p \leq 0.01$, and ***$p \leq 0.001$). (e) Schematic of EZHs with different network uniformities during stretching.

SBMAA) paired with slow crosslinkers (MBMA) produced more uniform structures. Therefore, when the reaction rates of the monomer and crosslinker are similar, they polymerize concurrently, generating networks with a more homogeneous molecular weight distribution. In contrast, large differences in reactivity lead to asynchronous polymerization, resulting in regions of long linear chains and localized crosslinker-rich clusters, thereby increasing the network heterogeneity.[47]

The crosslinking density, defined as the number of crosslinks per polymer volume fraction after swelling, includes both physical and chemical crosslinks. We compared the crosslinking densities (V_e) of EZHs with different network uniformities, and the results are shown in Fig. 3c. The more uniform EZHs exhibited higher crosslinking densities. This can be attributed to the fact that in non-uniform highly entangled networks, the physical entanglements are more prone to disentanglement during swelling, thereby reducing the effective crosslinking density.[29]

We next compared the elastic modulus of EZHs with different degrees of network uniformity. As shown in Fig. 3d, the results correlate strongly with the DLS measurements. The EZHs with more uniform networks exhibited a significantly higher elastic modulus, whereas those with heterogeneous net-

works demonstrated a weaker mechanical performance. Although the amount of chemical crosslinker in EZHs is extremely low, its influence is critical because the crosslinking points define the average polymer chain length between links, thereby affecting the mechanical behavior. As found in previous studies,[48] network uniformity impacts the elastic modulus of hydrogels. A uniform network reduces stress concentrations, leading to higher fracture strain and fracture energy, thereby enhancing the durability of the hydrogels. In addition, homogeneous networks contain fewer structural defects, such as dangling chains and excessive entanglements, which typically serve as sites for stress localization and mechanical failure in more heterogeneous networks (Fig. 3e).

Effect of network homogeneity on rheological properties

Rheological measurements were performed on a rotational rheometer by applying a series of shear strains to assess the viscoelastic behavior of the hydrogels. In this study, the MBAA crosslinker was used to develop ZHs and EZHs. As shown in Fig. 4a–d, ZHs exhibited a solid-like to liquid-like behavior at strain amplitudes of 250% to 500%, whereas EZHs underwent this transition at significantly lower strain amplitudes of 35% to 110%. The earlier transition in EZHs arises from their synthesis strategy, in which their increased chain entanglement enhances their viscosity and mechanical toughness while simultaneously facilitating chain mobility. Consequently, their liquid-like characteristics become more pronounced under deformation.[30]

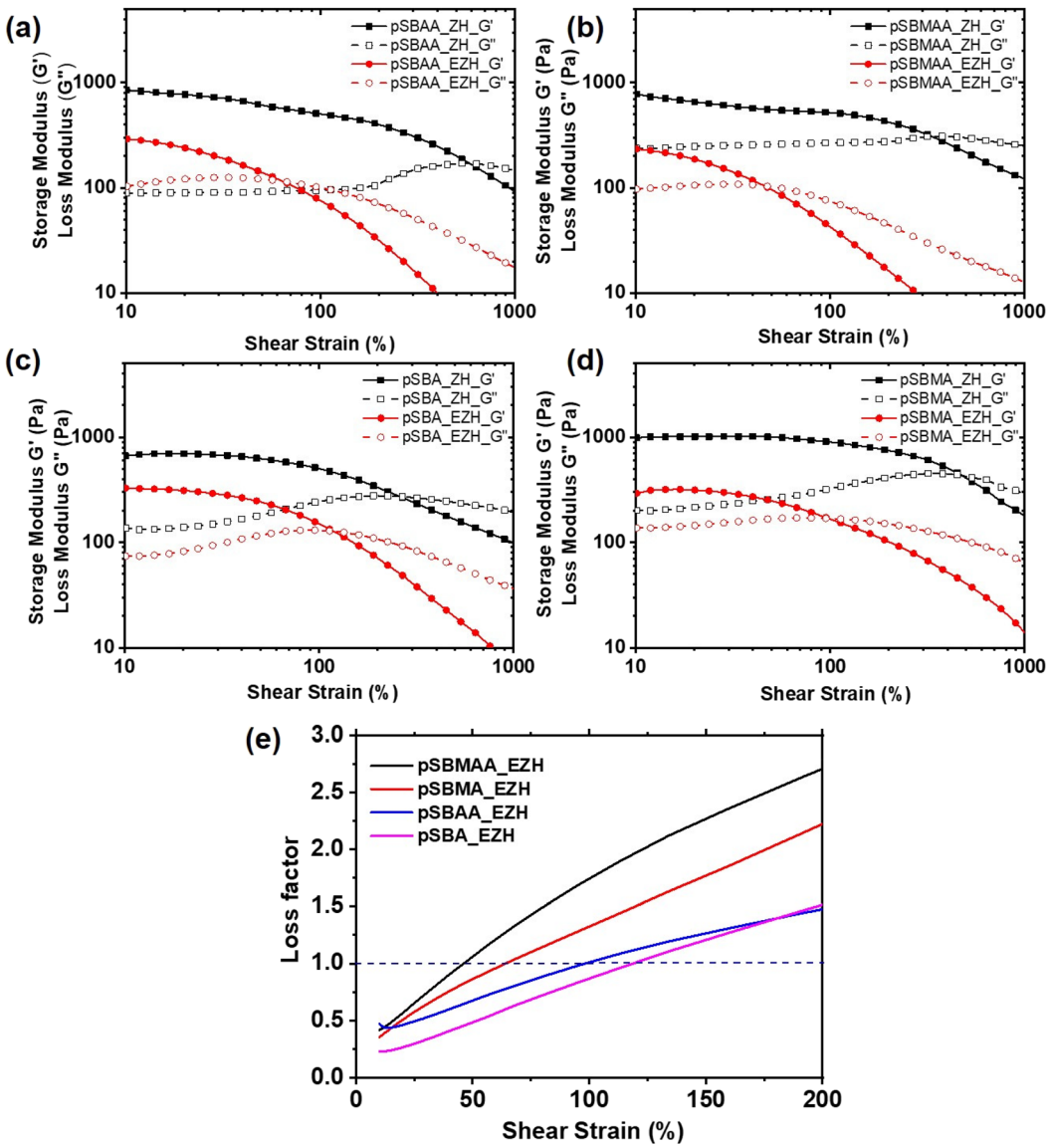

Fig. 4 Rheological measurements by applying a series of shear strains to assess the viscoelastic behavior of the ZHs and EZHs of pSBAA (a), pSBMAA (b), pSBA (c) and pSBMA (d). (e) Loss factors (tan δ) of the four EZHs.

In addition, we compared the loss factor (tan δ) of the four EZHs. As shown in Fig. 4e, the order in which tan δ reaches 1 is pSBMAA > pSBMA > pSBAA > pSBA. The hydrogels with a more heterogeneous network structure (pSBMAA and pSBMA) exhibit a faster increase in tan δ, demonstrating more prominent liquid-like behavior than the homogeneous networks of pSBAA and pSBA, respectively. This trend can be explained by the dynamic behavior of entangled chains under increasing strain. As the strain amplitude increases, the rate of disentanglement progressively accelerates and eventually surpasses the rate of re-entanglement. Hydrogels with broader molecular-weight distributions between chemical crosslinks exhibit more pronounced shear-thinning behavior, further enhancing their liquid-like characteristics.[49]

Surface property analysis

It has been shown that highly entangled non-ionic hydrogels, such as poly(acrylamide), exhibit enhanced lubrication due to their strong hydration and loosely packed surface chains.[28,45,50] However, the conformation and properties of polyelectrolytes and polyzwitterions are susceptible to the ionic strength in the solution.[50,51] Thus, to evaluate the effects of molecular structure and ionic strength on lubrication, we prepared EZHs and ZHs of pSBA with the crosslinker MBAA. As shown in Fig. 5a, the pSBA EZH exhibited poorer lubrication than the ZH in the same solution. Moreover, all the zwitterionic pSBA hydrogels showed lower friction in 0.15 M NaCl than that in DI water. Hydrogel lubrication is mainly influenced by (i) the conformation of the polymer chains on the surface and (ii) the surface energy.[50,52] Due to the anti-polyelectrolyte effect of zwitterionic polymers,[53] pSBA becomes more hydrated and swollen in the NaCl solution. Therefore, the results reflect that the zwitterionic hydrogels exhibited significantly enhanced lubrication under saline conditions. However, the lower lubrication of EZHs than ZHs could be attributed to their distinct surface adhesion energy.

We further analyzed the surface adhesion energy of the hydrogels using AFM and a contact mechanics model by analyzing the force–distance curves. As shown in Fig. 5b, the pSBA EZH exhibits markedly higher adhesion energy than the ZH. This result can be ascribed to the presence of abundant positively and negatively charged moieties within the 3D network, which result in a high dipole moment.[54,55] The substantial surface adhesion observed in EZHs explains, in part, their weaker lubrication performance.

To further evaluate and compare the macroscopic adhesion of EZHs and ZHs, we performed surface adhesion strength

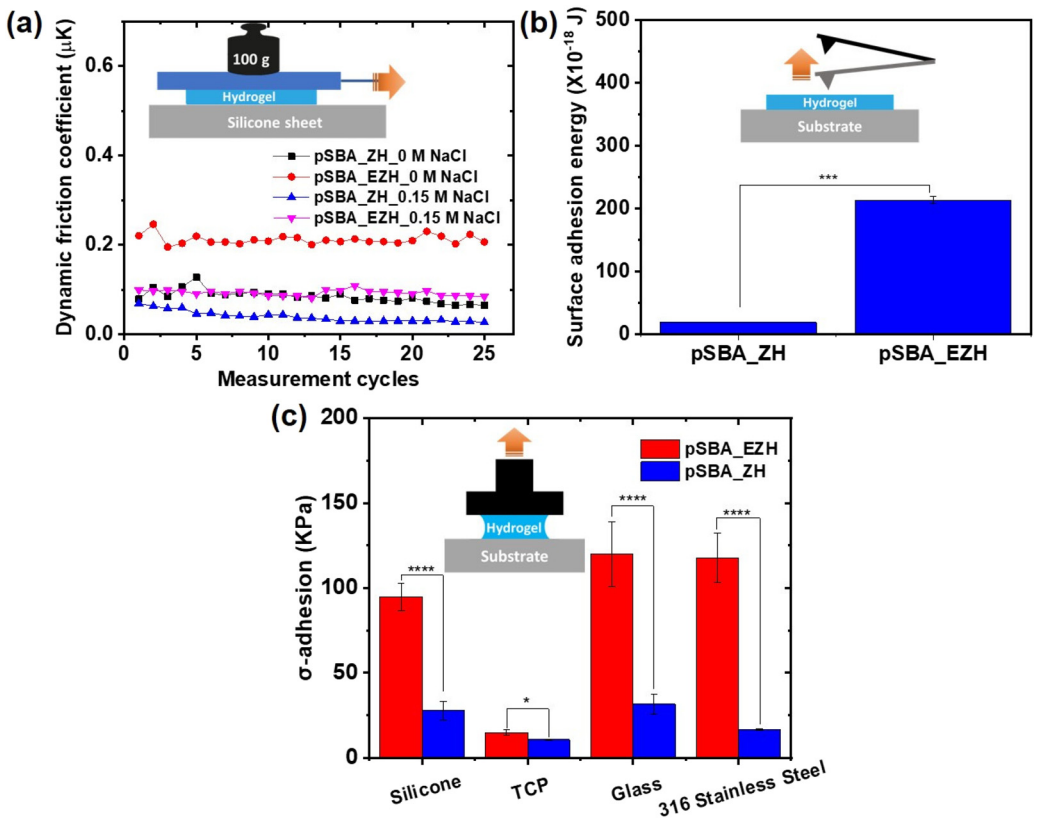

Fig. 5 (a) Lubrication tests for EZH and ZH of pSBA with crosslinker MBAA in fresh water and 0.15 M saline solution. (b) Surface adhesion energy of EZH and ZH of pSBA using AFM with a contact mechanics model. (c) σ-Adhesion strength tests for EZH and ZH of pSBA on silicone, TCP, 316 stainless steel, and glass substrates.

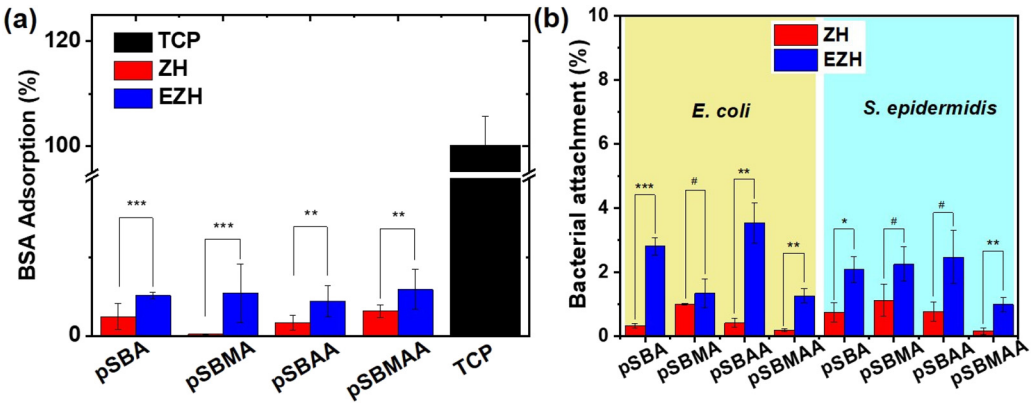

Fig. 6 (a) BSA adsorption on ZHs and EZHs of pSBA, pSBMA, pSBAA and pSBMAA relative to that on TCP. (b) Bacterial attachment of *E. coli* and *S. epidermidis* on ZHs and EZHs of pSBA, pSBMA, pSBAA and pSBMAA relative to attachment on TCP (n = 3; #p > 0.05, *$p \leq 0.05$, **$p \leq 0.01$, and ***$p \leq 0.001$).

tests on silicone, TCP, 316 stainless steel, and glass substrates (Fig. 5c). The σ-adhesion strength of EZHs on these substrates were higher than ZHs, which is consistent with the friction and AFM results (Fig. 5a and b, respectively) and reveals the higher surface energy of EZHs.

In adhesion-related evaluations, the key consideration is whether the hydrogel surface can effectively resist nonspecific adsorption. Therefore, we conducted both protein- and bacteria-adhesion experiments for ZHs and EZHs to compare their fouling resistance. Bovine serum albumin (BSA), the most abundant protein in blood, was used for evaluating anti-protein adsorption. As shown in Fig. 6a, all the ZHs and EZHs exhibited low BSA adsorption levels of <6% relative to that on TCP. Interestingly, the fouling levels of the EZHs prepared from different monomers were slightly higher than that of the ZHs.

For the antibacterial adhesion tests, Gram-negative *Escherichia coli* (*E. coli*) and Gram-positive *Staphylococcus epidermidis* (*S. epidermidis*) were used. The samples were observed under fluorescence microscopy after co-culture with bacteria and fluorescence staining and quantified using ImageJ. As shown in Fig. 6b, bacterial attachment on EZHs with respect to that on TCP ranged from 1.26%–3.5% for *E. coli* and 0.99%–2.25% for *S. epidermidis*. In contrast, ZHs showed lower attachment of 0.19%–1% for *E. coli* and 0.15%–1.12% for *S. epidermidis*.

Both the protein and bacterial adhesion results reveal a consistent trend that EZHs exhibit slightly compromised antifouling performance compared to the conventional ZHs. One possible explanation is that the loosely packed polymer network of the highly entangled hydrogels contains more nanoscale voids, allowing partial penetration of proteins or bacteria into the hydrogel matrix.[56] Another contributing factor may be the higher surface adhesion energy of EZHs, which increases their interfacial interactions relative to ZHs (Fig. 5b and c). Additionally, a previous study reported that densely packed zwitterionic chains can undergo intrachain associations,[57] reducing surface hydrophilicity and consequently weakening the antifouling performance.

Conclusions

In this study, we developed a highly entangled zwitterionic hydrogel platform and systematically examined how molecular structure, network uniformity, and intermolecular interactions influence hydration, mechanical properties, interfacial properties and fouling resistance. Using the optimized monomer ratio that maximizes chain entanglement, zwitterionic hydrogels from monomers (SBA, SBMA, SBAA and SBMAA) and crosslinkers (MBMA and MBAA) with distinct backbone substitution, reactivity and hydrogen bonding were synthesized to elucidate their key structure–property relationships. Mechanical testing revealed that EZHs lacking intermolecular hydrogen bonding (pSBA and pSBMA) exhibited greater mechanical enhancement than their hydrogen-bonded counterparts. Although hydrogen bonding is often expected to strengthen the polymer networks, in high-entanglement systems it instead increases hydration and swelling, giving rise to a low chain density and weakened entanglement-based reinforcement. The clear correlation between higher swelling ratios and reduced mechanical gains further confirms that chain entanglement is highly sensitive to the polymer chain density. Dynamic light scattering and tensile measurements showed that pairing monomers and crosslinkers with different reaction rates allows fine control over network homogeneity. The heterogeneous networks displayed lower stiffness and more pronounced shear-thinning behavior, whereas the more homogeneous architectures exhibited improved rigidity. All the EZHs demonstrated characteristic fluid-like responses, consistent with the dynamic nature of physical entanglements. Protein and bacterial adhesion experiments revealed a trade-off between bulk mechanical enhancement and surface antifouling behavior. Although chain entanglement significantly strengthened the zwitterionic hydrogels, their high surface energy and swelling-induced porous surface features allow biomolecules to diffuse and become temporarily trapped, reducing their antifouling efficiency. Overall, this work establishes chain entanglement as a robust strategy for enhancing the

toughness, strength, and energy dissipation of zwitterionic hydrogels. By tuning the monomer and crosslinker reactivity to control the network uniformity, the mechanical performance of these materials can be further tailored. These insights expand the design space of zwitterionic hydrogels and provide a foundation for developing next-generation materials for wearable devices, biomedical interfaces, and mechanically demanding environments.

Conflicts of interest

The authors declare no competing financial interest.

Data availability

All data underpinning this publication are available within the article and its associated supplementary information (SI). Supplementary information: synthesis routes for SBA, SBMA, SBAA and SBMAA, ^{1}H-NMR spectra of all monomers, schematic of the adhesion strength test and optimization of high toughness of EZHs with various cross-linking ratios. See DOI: https://doi.org/10.1039/d6lp00019c.

Acknowledgements

The authors acknowledge the National Science and Technology Council (NSTC 113-2811-E-008-009, 113-2918-I-008-004, 112-2221-E-008-007-MY3, 111-2628-E-008-003-MY3 and 111-2923-E-008-004-MY3) for financial support of this project.

References

1 J. Fu, Hydrogel properties and applications, *J. Mater. Chem. B*, 2019, **7**(10), 1523–1525.
2 S. T. Dong, S. H. An, Q. Saiding, Q. Chen, B. Liu, N. Kong, W. Chen and W. Tao, Therapeutic Hydrogels: Properties and Biomedical Applications, *Chem. Rev.*, 2025, **125**(18), 8835–8920, DOI: 10.1021/acs.chemrev.5c00182.
3 K. Ishihara, Advances in bioinspired polymer hydrogel systems with biomedical functionalities, *Sci. Technol. Adv. Mater.*, 2025, **26**(1), 2469490, DOI: 10.1080/14686996.2025.2469490.
4 R. J. Song, X. Y. Wang, M. Johnson, C. Milne, A. Lesniak-Podsiadlo, Y. H. Li, J. Lyu, Z. S. Li, C. Y. Zhao, L. Z. Yang, *et al.*, Enhanced Strength for Double Network Hydrogel Adhesive Through Cohesion-Adhesion Balance, *Adv. Funct. Mater.*, 2024, **34**(23), 2313322, DOI: 10.1002/adfm.202313322.
5 X. Y. Li and J. P. Gong, Design principles for strong and tough hydrogels, *Nat. Rev. Mater.*, 2024, **9**(6), 380–398, DOI: 10.1038/s41578-024-00672-3.
6 Y. C. Zhang, Q. Chen, Z. W. Dai, Y. Dai, F. Xia and X. J. Zhang, Nanocomposite adhesive hydrogels: from design to application, *J. Mater. Chem. B*, 2021, **9**(3), 585–593, DOI: 10.1039/d0tb02000a.
7 D. D. Tian, W. J. Ma, L. J. Zheng, K. X. Jiang, H. He and R. Y. Sun, Tough, Healable, Photoresponsive Actuator Based on a Quadruple Hydrogen-Bond-Capped Slide-Ring Structure, *ACS Appl. Polym. Mater.*, 2023, **5**(10), 8641–8649, DOI: 10.1021/acsapm.3c01683.
8 H. Xiao, X. T. Lai, X. R. Xiong, Z. T. Jiang, Y. G. Jia, H. Liu, W. Huang, G. Wu and X. X. Zhu, Double-Network Slide-Ring Topological Hydrogel Fibers: Fabrication and Sensor Application, *Small*, 2025, **21**(18), 2501558, DOI: 10.1002/smll.202501558.
9 F. Di Lorenzo and S. Seiffert, Nanostructural heterogeneity in polymer networks and gels, *Polym. Chem.*, 2015, **6**(31), 5515–5528, DOI: 10.1039/c4py01677g.
10 M. X. Wang, J. Hu and M. D. Dickey, Emerging applications of tough ionogels, *NPG Asia Mater.*, 2023, **15**(1), 66, DOI: 10.1038/s41427-023-00514-8.
11 J. Kim, G. G. Zhang, M. X. Shi and Z. G. Suo, Fracture, FaZtigue, and friction of polymers in which entanglements greatly outnumber cross-links, *Science*, 2021, **374**(6564), 212–216, DOI: 10.1126/science.abg6320.
12 C. Norioka, Y. Inamoto, C. Hajime, A. Kawamura and T. Miyata, A universal method to easily design tough and stretchable hydrogels, *NPG Asia Mater.*, 2021, **13**(1), 34, DOI: 10.1038/s41427-021-00302-2.
13 L. M. Kong, J. Q. Zhang, S. Q. Huang, R. C. Zhang, J. M. Li, Z. T. Xie and J. R. Wu, Designing Highly Entangled, Homogeneous, and Low-Defect Networks for High-Performance Rubbers, *Macromolecules*, 2025, **58**(6), 3109–3118, DOI: 10.1021/acs.macromol.4c03133.
14 L. H. Rong, J. V. M. Madayag, J. Ge, T. Q. Guan and E. B. Caldona, Highly Entangled Polymer Gels Toward Controlled Stiffness and Toughness in Soft Materials, *Polym. Rev.*, 2025, **66**(1), 1–35, DOI: 10.1080/15583724.2025.2580645.
15 X. Y. He, P. G. Ma, S. Ma, R. Z. Cao, J. Li, Y. Y. Lu, Y. L. Liang, X. Tian, Z. Q. Wang and X. Q. Lu, Super-stretchable, freezing-resistant and self-powered organohydrogels for extreme environment-adaptable high-performance strain sensors, *Nanoscale*, 2025, **17**(18), 11450–11460, DOI: 10.1039/d5nr00962f.
16 J. W. Wang, Q. Shao, W. W. Wang, Z. Y. Ma, L. X. Wu, R. Q. Song, H. M. Liang, Y. X. Dong, M. Tahir, Z. L. Hu, *et al.*, Enhancing the performance of hydrogel strain/pressure sensors via gradient-entanglement-induced surface wrinkling patterns, *Chem. Eng. J.*, 2024, **498**, 155679, DOI: 10.1016/j.cej.2024.155679.
17 É. Ansart, L. Cousin, M. W. Tibbitt and S. Mommer, Enhanced toughness in highly entangled hydrogels via non-covalent molecular hooks, *Mater. Horiz.*, 2026, **13**, 940–947, DOI: 10.1039/d5mh01344e.
18 X. Z. Song, J. Man, X. J. Wang, J. L. Wang, Y. Q. Zhang, J. Y. Li, J. F. Li and Y. G. Chen, Pure Zwitterionic Hydrogels with High Entanglement Reinforcement for Biomedical Applications, *ACS Appl. Mater. Interfaces*, 2025, **17**(34), 48094–48110, DOI: 10.1021/acsami.5c12081.

19 L. X. Wei, Y. Yang, X. Y. Qiu, J. Shen, Y. M. Zhao, X. L. Zhang, B. H. Hu, T. Yang, H. C. Fu, S. Chen, *et al.*, Self-Polymerized Tough and High-Entanglement Zwitterionic Functional Hydrogels, *Small*, 2024, **20**(50), 2405789, DOI: 10.1002/smll.202405789.

20 H. L. Bui, H. N. Nguyen, J. Y. Lai and C. J. Huang, Engineering principles of zwitterionic hydrogels: Molecular architecture to manufacturing innovations for advanced healthcare materials, *Mater. Today Bio*, 2025, **33**, 102085, DOI: 10.1016/j.mtbio.2025.102085.

21 L. R. Gao, A. Varley, H. Gao, B. W. Li and X. H. Li, Zwitterionic Hydrogels: From Synthetic Design to Biomedical Applications, *Langmuir*, 2025, **41**(5), 3007–3026, DOI: 10.1021/acs.langmuir.4c04788.

22 C. T. V. Nguyen, S. K. K. Chow, H. N. Nguyen, T. S. Liu, A. Walls, S. Withey, P. Liebig, M. Mueller, B. Thierry, C. T. Yang, *et al.*, Formation of Zwitterionic and Self-Healable Hydrogels via Amino-yne Click Chemistry for Development of Cellular Scaffold and Tumor Spheroid Phantom for MRI, *ACS Appl. Mater. Interfaces*, 2024, **16**(28), 36157–36167, DOI: 10.1021/acsami.4c06917.

23 K. T. Huang, W. H. Hung, Y. C. Su, F. C. Tang, L. D. Linh, C. J. Huang and L. H. Yeh, Zwitterionic Gradient Double-Network Hydrogel Membranes with Superior Biofouling Resistance for Sustainable Osmotic Energy Harvesting, *Adv. Funct. Mater.*, 2023, **33**(19), 2211316, DOI: 10.1002/adfm.202211316.

24 X. H. Zhao, X. Y. Chen, H. Yuk, S. T. Lin, X. Y. Liu and G. Parada, Soft Materials by Design: Unconventional Polymer Networks Give Extreme Properties, *Chem. Rev.*, 2021, **121**(8), 4309–4372, DOI: 10.1021/acs.chemrev.0c01088.

25 D. L. Safranski and K. Gall, Effect of chemical structure and crosslinking density on the thermo-mechanical properties and toughness of (meth)acrylate shape memory polymer networks, *Polymer*, 2008, **49**(20), 4446–4455, DOI: 10.1016/j.polymer.2008.07.060.

26 S. Ida, D. Nishisako, A. Fujiseki and S. Kanaoka, Thermoresponsive properties of polymer hydrogels induced by copolymerization of hydrophilic and hydrophobic monomers: comprehensive study of monomer sequence and water affinity, *Soft Matter*, 2021, **17**(25), 6063–6072, DOI: 10.1039/D1SM00596K.

27 T. Masuda, Y. Saegusa, T. Tsuji and M. Takai, Development of deformable and adhesive biocompatible polymer hydrogels by a simple one-pot method using ADIP as a cationic radical initiator, *Polym. J.*, 2025, **57**(11), 1257–1268, DOI: 10.1038/s41428-025-01025-9.

28 J. Kim, G. Zhang, M. Shi and Z. Suo, Fracture, fatigue, and friction of polymers in which entanglements greatly outnumber cross-links, *Science*, 2021, **374**(6564), 212–216.

29 C. Norioka, A. Kawamura and T. Miyata, Relatively homogeneous network structures of temperature-responsive gels synthesized via atom transfer radical polymerization, *Soft Matter*, 2023, **19**(14), 2505–2513.

30 C. Norioka, Y. Inamoto, C. Hajime, A. Kawamura and T. Miyata, A universal method to easily design tough and stretchable hydrogels, *NPG Asia Mater.*, 2021, **13**(1), 34.

31 T. Miyata, A. Jikihara, K. Nakamae and A. S. Hoffman, Preparation of poly(2-glucosyloxyethyl methacrylate)concanavalin A complex hydrogel and its glucose-sensitivity, *Macromol. Chem. Phys.*, 1996, **197**(3), 1135–1146, DOI: 10.1002/macp.1996.021970330.

32 J. L. Hutter and J. Bechhoefer, Calibration of atomic–force microscope tips, *Rev. Sci. Instrum.*, 1993, **64**(7), 1868–1873.

33 L. Gong, L. Xiang, J. Zhang, J. Chen and H. Zeng, Fundamentals and advances in the adhesion of polymer surfaces and thin films, *Langmuir*, 2019, **35**(48), 15914–15936.

34 S. Vlassov, S. Oras, M. Antsov, I. Sosnin, B. Polyakov, A. Shutka, M. Y. Krauchanka and L. M. Dorogin, Adhesion and mechanical properties of PDMS-based materials probed with AFM: A review, *Rev. Adv. Mater. Sci.*, 2018, **56**(1), 62–78.

35 H. You, S. J. Zheng, H. Li and K. Y. Lam, A model with contact maps at both polymer chain and network scales for tough hydrogels with chain entanglement, hidden length and unconventional network topology, *Int. J. Mech. Sci.*, 2024, **262**, 108713, DOI: 10.1016/j.ijmecsci.2023.108713.

36 M. A. Ramin, G. Le Bourdon, K. Heuze, M. Degueil, T. Buffeteau, B. Bennetau and L. Vellutini, Epoxy-terminated self-assembled monolayers containing internal urea or amide groups, *Langmuir*, 2015, **31**(9), 2783–2789.

37 A. Buckingham, J. Del Bene and S. McDowell, The hydrogen bond, *Chem. Phys. Lett.*, 2008, **463**(1–3), 1–10.

38 S. Horowitz and R. C. Trievel, Carbon-oxygen hydrogen bonding in biological structure and function, *J. Biol. Chem.*, 2012, **287**(50), 41576–41582.

39 T. Steiner, The hydrogen bond in the solid state, *Angew. Chem., Int. Ed.*, 2002, **41**(1), 48–76.

40 H. Chavda and C. Patel, Effect of crosslinker concentration on characteristics of superporous hydrogel, *Int. J. Pharm. Invest.*, 2011, **1**(1), 17.

41 W. Xue, S. Champ and M. B. Huglin, Network and swelling parameters of chemically crosslinked thermoreversible hydrogels, *Polymer*, 2001, **42**(8), 3665–3669.

42 X. Liu, Q. Zhang, F. Jia and G. Gao, Underwater flexible mechanoreceptors constructed by anti-swelling self-healable hydrogel, *Sci. China Mater.*, 2021, **64**, 3069–3078.

43 F. Wu, Y. Pang and J. Liu, Swelling-strengthening hydrogels by embedding with deformable nanobarriers, *Nat. Commun.*, 2020, **11**(1), 4502.

44 Y. He, H.-K. Tsao and S. Jiang, Improved mechanical properties of zwitterionic hydrogels with hydroxyl groups, *J. Phys. Chem. B*, 2012, **116**(19), 5766–5770.

45 I. Lacík, A. Chovancová, L. Uhelská, C. Preusser, R. A. Hutchinson and M. Buback, PLP-SEC studies into the propagation rate coefficient of acrylamide radical polymerization in aqueous solution, *Macromolecules*, 2016, **49**(9), 3244–3253.

46 C. S. Brazel and S. L. Rosen, *Fundamental principles of polymeric materials*, John Wiley & Sons, 2012.

47 G. Patras, G. G. Qiao and D. H. Solomon, Controlled formation of microheterogeneous polymer networks: Influence of monomer reactivity on gel structure, *Macromolecules*, 2001, **34**(18), 6396–6401.
48 M. Tosa, K. Hashimoto, H. Kokubo, K. Ueno and M. Watanabe, Effect of network homogeneity on mechanical, thermal and electrochemical properties of solid polymer electrolytes prepared by homogeneous 4-arm poly (ethylene glycols), *Soft Matter*, 2020, **16**(17), 4290–4298.
49 M. P. Stevens, *Polymer chemistry*, Oxford university press, New York, 1990.
50 J. P. Gong, Friction and lubrication of hydrogels—its richness and complexity, *Soft Matter*, 2006, **2**(7), 544–552.
51 Q. S. Li, C. Y. Wen, J. Yang, X. C. Zhou, Y. N. Zhu, J. Zheng, G. Cheng, J. Bai, T. Xu, J. Ji, *et al.*, Zwitterionic Biomaterials, *Chem. Rev.*, 2022, **122**(23), 17073–17154, DOI: 10.1021/acs.chemrev.2c00344.
52 A. A. Pitenis, J. Manuel Urueña, R. M. Nixon, T. Bhattacharjee, B. A. Krick, A. C. Dunn, T. E. Angelini and W. Gregory Sawyer, Lubricity from entangled polymer networks on hydrogels, *J. Tribol.*, 2016, **138**(4), 042102.
53 F. Wang, J. Yang and J. Zhao, Understanding anti–polyelectrolyte behavior of a well–defined polyzwitterion at the single–chain level, *Polym. Int.*, 2015, **64**(8), 999–1005.
54 Y. Sun, S. Lu, Q. Li, Y. Ren, Y. Ding, H. Wu, X. He and Y. Shang, High strength zwitterionic nano-micelle hydrogels with superior self-healing, adhesive and ion conductive properties, *Eur. Polym. J.*, 2020, **133**, 109761.
55 T. Xu, L. Zhang, B. Song, X. Bai, Z. Huang, X. Bu, T. Chen, H. Fu and P. Guo, High-strain sensitive zwitterionic hydrogels with swelling-resistant and controllable rehydration for sustainable wearable sensor, *J. Colloid Interface Sci.*, 2022, **620**, 14–23.
56 W. Yang, T. Bai, L. R. Carr, A. J. Keefe, J. Xu, H. Xue, C. A. Irvin, S. Chen, J. Wang and S. Jiang, The effect of lightly crosslinked poly (carboxybetaine) hydrogel coating on the performance of sensors in whole blood, *Biomaterials*, 2012, **33**(32), 7945–7951.
57 O. Azzaroni, A. A. Brown and W. T. Huck, UCST wetting transitions of polyzwitterionic brushes driven by self–association, *Angew. Chem., Int. Ed.*, 2006, **45**(11), 1770–1774.